type of hypothesis test used and the method of computation employed. In unfavourable circumstances the validity of the test may be totally nullified.

In reporting the results of crystal-structure analyses it is conventional to follow each atomic coordinate and temperature factor by its e.s.d. Usually this is given in brackets in the units of the least significant digit of the coordinate or temperature factor. Our results suggest that serious round-off errors in inter-experimental comparisons only occur when this number in brackets is small, *i.e.* 1, 2 and, possibly, 3. Thus, the problems discussed in this paper can be overcome if an extra digit of significance is reported in these cases.

Olga Kennard is a member of the external staff of the Medical Research Council.

References

ABRAHAMS, S. C. & KEVE, E. T. (1971). *Acta Cryst.* A**27**, 157-165.
HAMILTON, W. C. (1964). *Statistics in Physical Science*, pp. 46-47. New York: Ronald Press.
HAMILTON, W. C. (1969). *Acta Cryst.* A**25**, 194-206.
HAMILTON, W. C. & ABRAHAMS, S. C. (1972). *Acta Cryst.* A**28**, 215-218.
MASSEY, F. J. JR (1951). *J. Am. Stat. Assoc.* **46**, 68-78.
NAG Fortran Library Manual (1983). Mark 10, Vol. 5.
SIEGEL, S. (1956). *Nonparametric Statistics for the Behavioral Sciences.* Tokyo: McGraw-Hill Kogakusha.

Acta Cryst. (1985). A**41**, 128-133

Simulation of Multiple Diffraction

BY Y. SOEJIMA AND A. OKAZAKI

Department of Physics, Kyushu University, Fukuoka 812, *Japan*

AND T. MATSUMOTO

Department of Earth Sciences, Kanazawa University, Kanazawa 920, *Japan*

(*Received* 27 *April* 1984; *accepted* 1 *August* 1984)

Abstract

The multiple diffraction of X-rays and neutrons is discussed on the basis of the kinematical theory; a program for the simulation of ψ scanning and λ scanning is developed, where the influence of the wavelength width of incident beams on the Ewald construction is properly taken into account. The effect of higher-order diffraction (n-beam interaction, $n>3$) is treated as the sum of those of $(n-2)$ pairs of relevant double diffractions (three-beam interactions). Applications are made for some examples for which experimental data are available; it is shown that the results are in very good agreement with experiment. This suggests that the kinematical approach is appropriate. The simulation is useful in planning ψ-scanning experiments for precise structure determination and for examining experimental data.

1. Introduction

Since Renninger (1937) showed the phenomenon of double diffraction (*Umweganregung*) in the pattern of ψ scanning of 222 of diamond, the importance of the effect on structure determinations has often been discussed. In the early days, discussions were mainly concerned with possible errors in space-group determination because, as mentioned by Lipson & Cochran (1953), the effect can interfere with the detection of glide planes and screw axes. Later, in connection with precise structure determination, the effect has been considered more generally (Coppens, 1968; Panke & Wölfel, 1968): its effect on general reflections has been considered, to improve the accuracy of the intensity.

The ψ-scanning experiment, on the other hand, is not very easy even at present, particularly with specimens in special environments such as low or high temperature; it also requires a long machine time. If a computer simulation is available for double (*i.e.* multiple) diffraction, it will therefore be very useful in planning the ψ-scanning experiment. Moreover, in some cases, the experiment will be replaced by such a simulation, in part at least. Examination of the results of the ψ-scanning data by comparison with the simulation will also be worth doing.

In the following, a computer simulation based on the kinematical theory will be developed for ψ scanning with monochromatic incident beams and for λ scanning with white beams. The results will be applied to some examples and compared with experiments.

0108-7673/85/020128-06$01.50

2. Formulation

2.1. *Geometrical condition*

An Ewald construction for double diffraction (three-beam interaction) is shown in Fig. 1, where the reciprocal-lattice point being examined is labelled **h**; the second reciprocal-lattice point on the Ewald sphere, called an operative point, is labelled $\mathbf{h}_{op}$. If there are two or more operative points, they will be indexed by an additional integer suffix. (See Appendix *A*.)

We take the influence of the wavelength widths of the incident beams into account. In this case, the Ewald sphere can be defined by a pair of spheres, touching each other at the point *O*, with radii corresponding to the wavelengths $\lambda+\Delta\lambda$ and $\lambda-\Delta\lambda$. We then put the point **h** in the middle of the thickness of the sphere, the position for λ. In Fig. 2, a section of the spheres including the point $\mathbf{h}_{op}$ together with the wavevector of the incident beams is shown with an exaggerated thickness. The thickness Δl along the radial direction $\mathbf{h}_{op}$ is given by

$$\Delta l = 2\left(\frac{1}{\lambda-\Delta\lambda}-\frac{1}{\lambda+\Delta\lambda}\right)\cos\alpha = \frac{4\Delta\lambda}{\lambda^2-(\Delta\lambda)^2}\cos\alpha, \tag{1}$$

where α is the angle shown in the figure. Reciprocal-lattice points for which the condition

$$\left|\,|\mathbf{h}_{op}|-\frac{2}{\lambda}\cos\alpha\,\right| \le \frac{\Delta l}{2} \tag{2}$$

is fulfilled will be regarded as operative points.

As seen in Fig. 2, the thickness of the sphere is rather sensitive to the Bragg angle θ. If t denotes the thickness along the direction of the wavevector of the scattered beams for λ,

$$t \simeq \frac{4\Delta\lambda}{\lambda^2-(\Delta\lambda)^2}\sin^2\theta. \tag{3}$$

The ratio of t's at $\theta=45$ and 10° is about 17:1.

For ψ scanning, the Ewald sphere is rotated stepwise about the vector **h**, while, for λ scanning, the radius of the sphere is varied stepwise keeping the point **h** stationary. The conventional procedure is followed for these calculations.

2.2. *Intensity*

Here we introduce a reciprocal-lattice point called the cooperative point; it is represented by a vector $\mathbf{h}_{co}$ in Fig. 1 and defined by the relation

$$\mathbf{h} = \mathbf{h}_{op} + \mathbf{h}_{co}. \tag{4}$$

The quantities concerned with **h**, $\mathbf{h}_{op}$ and $\mathbf{h}_{co}$ will be indicated by the suffixes **h**, op and co, respectively.

The present intensity calculation follows the treatment in the kinematical theory. We start from the expression for the intensity at **h** when no multiple diffraction occurs. It will be denoted by $I_{\mathbf{h}}$ and given by

$$I_{\mathbf{h}} = I_0 r_{\mathbf{h}} N_{\mathbf{h}}, \tag{5}$$

where I_0 is the incident intensity and $r_{\mathbf{h}}$ an effective reflectivity including absorption and extinction, while

$$N_{\mathbf{h}} = |F_{\mathbf{h}}|^2 \mathrm{Lp}. \tag{6}$$

On the right-hand side, conventional notations are used; for neutron diffraction, the Lp factor will be replaced by the Lorentz factor. The Lorentz and polarization factors for three-beam cases given respectively by Post (1975) and Zachariasen (1965) will be used in the following. For the latter, the detail is given in Appendix *B*. The $N_{\mathbf{h}}$'s are normalized to the largest among them.

When the geometrical condition for three-beam interaction is fulfilled by **h** and $\mathbf{h}_{op}$, the intensity diffracted towards these points after the first (or primary) diffraction, $I_{\mathbf{h}}$ and I_{op} respectively (Fig. 1), can be given by

$$I_{\mathbf{h}} = (I_0 - I_{op}) r_{\mathbf{h}} N_{\mathbf{h}} \tag{7a}$$

$$I_{op} = (I_0 - I_{\mathbf{h}}) r_{op} N_{op}. \tag{7b}$$

We understand that we observe intensities at **h** and $\mathbf{h}_{op}$, which correspond to effective incident intensities

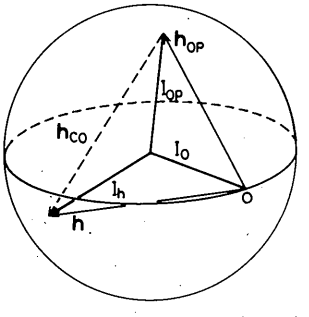

Fig. 1. Ewald construction for double diffraction (three-beam interaction). **h**, $\mathbf{h}_{op}$ and $\mathbf{h}_{co}$, respectively, denote the reciprocal-lattice point being examined, operative point and cooperative point defined by (4). Flow of intensity is shown as well.

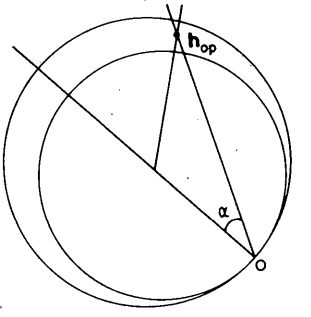

Fig. 2. Schematic representation of the effect of $\Delta\lambda$, the width of the wavelength of the incident beam, on the Ewald construction for the three-beam case.

$I_0 - I_{op}$ and $I_0 - I_h$ respectively. The solution of the simultaneous equations gives I_h and I_{op}:

$$I_h = \frac{r_h N_h (1 - r_{op} N_{op})}{1 - r_h r_{op} N_h N_{op}} I_0 \qquad (8a)$$

$$I_{op} = \frac{r_{op} N_{op} (1 - r_h N_h)}{1 - r_h r_{op} N_h N_{op}} I_0. \qquad (8b)$$

Since the order of magnitude of r's is $\sim 10^{-2}$-10^{-3}, the denominators of (8) can be approximated to unity.

We represent the intensity actually observed at **h** by $(I_h)_{obs}$, which will be given by I_h in (8*a*) after correcting for the intensity escaping to $\mathbf{h}_{op}$ *via* $\mathbf{h}^*_{co}$, and for that coming from $\mathbf{h}_{op}$ *via* $\mathbf{h}_{co}$. The two cooperative points form a Friedel pair; thus $\mathbf{h}^*_{co} = -\mathbf{h}_{co}$. We then get the following relation:

$$\begin{aligned}(I_h)_{obs}/I_0 \simeq\ & r_h N_h (1 - r_{op} N_{op}) \\ & - r_h N_h (1 - r_{op} N_{op}) r^*_{co} N^*_{co} \\ & + r_{op} N_{op} (1 - r_h N_h) r_{co} N_{co}. \end{aligned} \qquad (9)$$

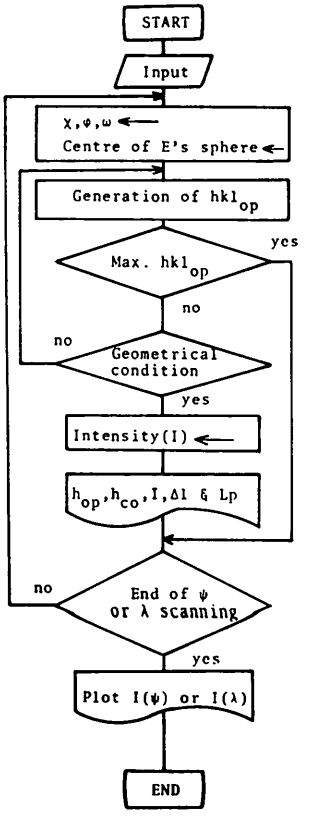

Fig. 3. Flow chart for simulating multiple diffraction. The input parameters include lattice constants, structural parameters, λ, $\Delta\lambda$, r, I_0, domain distribution parameters, crystal alignment parameters, and specifications of **h**, X-ray or neutron and ψ or λ scanning.

Except in the region of anomalous dispersion, $N_{co} = N^*_{co}$. Moreover, in the present calculation, we start assuming that the reflectivity is constant for any reflection. Under these conditions, we find that

$$\begin{aligned}(I_h)_{obs}/I_0 = {} & rN_h(1 - rN_{op}) \\ & - r^2 N_h N_{co} + r^2 N_{op} N_{co}. \end{aligned} \qquad (10)$$

This expression is essentially equivalent to those given by Moon & Shull (1964) and Coppens (1968). The corrections for I_h with positive and negative signs correspond to the processes of *Umweganregung* and *Aufhellung*, respectively.

From (10), we wee that the effect of three-beam interaction will be most remarkable if $N_h \simeq 0$ and both of N_{op} and N_{co} are large (Coppens, 1968). Then *Umweganregung* is dominant and

$$(I_h)_{obs}/I_0 \simeq r^2 N_{op} N_{co}. \qquad (11)$$

On the other hand, if N_{op} (or N_{co}) $\simeq 0$ and N_{co} (or N_{op}) is large, *Aufhellung* is dominant, though the effect will be much less appreciable:

$$(I_h)_{obs}/I_0 \simeq rN_h(1 - rN_{co}), \qquad (12a)$$

or

$$(I_h)_{obs}/I_0 \simeq rN_h(1 - rN_{op}). \qquad (12b)$$

Aufhellung will also be dominant if $N_h \simeq N_{op}$ (or $N_h \simeq N_{co}$). We then find

$$(I_h)_{obs}/I_0 \simeq rN_h(1 - rN_h). \qquad (13)$$

The effect of possible multiple diffractions (n-beam cases) due to the existence of two or more operative points can be regarded, as given in Appendix *A*, as the effect of a whole set of three-beam interactions including **h** and one of the operative points.

A few examples of the simulation, which follows the procedure mentioned above, will be presented in the following; a flow chart for the calculation is shown in Fig. 3.

3. Applications

3.1. CaF_2

In the upper part of Fig. 4, the simulation of ψ scanning of 002 of CaF_2 with Mo $K\alpha$ radiation is shown, where the calculation is made for $\Delta\lambda/\lambda = 0{\cdot}1\%$, $r = 0{\cdot}02\%$, $B_{Ca} = B_F = 1$ Å^2 and steps of $\psi = 0{\cdot}05°$. In the lower part, on the other hand, the experimental results given by Coppens (1968)* are shown upside-down, where the ψ step is 0·04°.

* No description of the radiation used is given in the reference. The present assignment is made, after examining several characteristic X-rays usually used, as the only one that gave reasonable agreement with the experiment.

The intensity of 002 is extremely weak, although not zero, even among the weak reflections with $h+k+l=4n+2$. It is so weak that the effect of the n-beam interaction can be observed fairly clearly. In this situation, we can determine the value of r by normalizing the intensity of n-beam interactions to that of 002, the constant intensity in the figure. The value mentioned above has been determined in this way.

The overall agreement observed suggests that the present treatment as well as the assumptions included are reasonable. Moreover, it may be worth mentioning that the peak at $\psi=23°$ consists of six three-beam components; all of them have weak contributions resulting from operative and cooperative reflections with h, k, l all even. One of the largest contributions, about a third of the total intensity, is due to the pair $0\bar{2}\bar{2}$ and 024; the former is very strong and the latter weak. The ratio of the values of $|F|^2$ for $0\bar{2}\bar{2}$, 024 and 002 is about 33 000:210:1. That is, although both 024 and 002 belong to the same group with $h+k+l=4n+2$, the latter is very much weaker than the former. This is the situation in which the three-beam interaction involving a weak reflection is appreciable for a weak **h**.

3.2. *Hypersthene*

More precise ψ scans have been carried out for hypersthene with space group *Pbca* (Sasaki & Matsumoto, 1977; Sasaki, Matsumoto & Sawada, 1981; Matsumoto, 1983). In Fig. 5, the experimental data for 071 with Mo $K\alpha$ are shown in the lower part, while in the upper part the simulation is shown. In this calculation, the observed intensity data set for stronger 205 reflections is directly used instead of calculating from the structural parameters; $\Delta\lambda/\lambda=0{\cdot}1\%$ and the step of ψ is 0·125°. The value of r is taken to be 0·5%, although it will be meaningful only when the intensity is compared with that of symmetrically allowed reflections. In this figure, we find very good agreement between the simulation and the experiment. Minor disagreements seen there can be attributed to errors in calculation, namely those due to the use of an incomplete intensity data set and of the ψ step, which is not small enough; experimental errors may in part be responsible for the disagreements.

3.3. GaAs

Another precise example has been given for 002 of GaAs (Chang & Post, 1975); the ψ-scanning pattern and the simulation are shown in Fig. 6. The agreement is again excellent.

3.4. *Others*

In addition to the cases mentioned above, the simulation has been applied to a few more examples including those of the λ scanning; a list is given in Table 1 together with those mentioned above. No serious discrepancy has been observed between the simulation and the experiment, except for the case of $MgAl_2O_4$ (Thompson & Grimes, 1977); in this particular case, the calculation given by the authors is not in agreement with the experiment. In the case of Fe_3O_4, magnetic components of the intensity are taken into account in the simulation.

4. Discussion

As pointed out by Lipson & Cochran (1953), the effect of double diffractions cannot produce any uncertainty

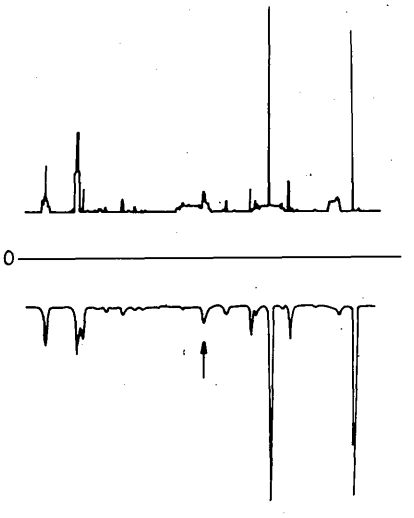

Fig. 4. Pattern of ψ scanning for 002 of CaF_2 with Mo $K\alpha$. The upper part is that of the present simulation and lower part that of the experiment (Coppens, 1968). The peak at $\psi=23°$ mentioned in the text is marked by an arrow.

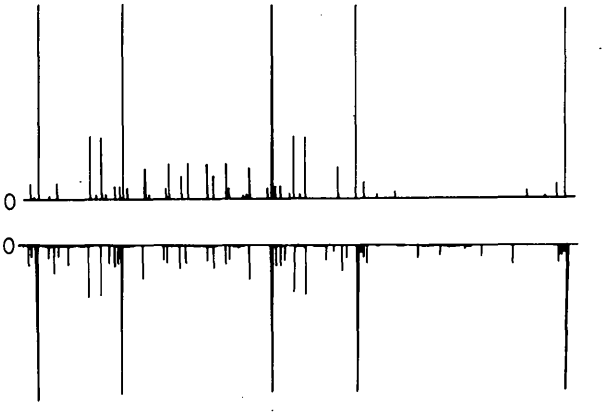

Fig. 5. Pattern of ψ scanning for 071 of hypersthene with Mo $K\alpha$. The lower part is that of the experiment (Sasaki & Matsumoto, 1977; Matsumoto, 1983).

Table 1. *A list of examples for which comparison with the present simulation has been made*

Material	*hkl*	Beam	Type of scan	Reference
CaF_2	002	X-ray (Mo $K\alpha$)	ψ	Coppens (1968)
Ge	222	X-ray (Cu $K\alpha_1$)	ψ	Post (1975)
GaAs	002	X-ray (Cu $K\alpha_1$)	ψ	Chang & Post (1975)
Hypersthene	071, 900, 10,0,0	X-ray (Mo $K\alpha$)	ψ	Sasaki & Matsumoto (1977) Matsumoto (1983)
Fe_3O_4	200	Neutron	ψ	Samuelson (1974)*
	402	Neutron	λ	Shirane *et al.* (1975)
	200	Neutron	λ, ψ	
$MgAl_2O_4$	200	Neutron	ψ	Samuelson & Steinsvoll (1975)†
	200	Neutron	ψ	Thompson & Grimes (1977)

* The peaks in Fig. 1 of the reference are assigned to double diffraction of the type {311}-{111}. On the contrary, the present calculation shows that the main contributions to the peaks at $\psi \simeq 4$ and 7° are due to {331}-{333} and {311}-{311}, respectively. The contribution of {311}-{111} appears on the peak at $\psi \simeq 12°$, outside the range of the figure.

† The peak at $\psi \sim 10°$ in Fig. 1 of this reference is assigned to the double diffraction {311}-{111}. The present calculation shows that the contribution of this is negligible because of very much weaker intensity of {111} in contrast to the case of Fe_3O_4. The main contribution to the peak is due to {311}-{311} instead.

of lattice type, *P, I, F etc.* This can readily be understood by looking at the following form of (4):

$$\begin{pmatrix} h \\ k \\ l \end{pmatrix}_h = \begin{pmatrix} h \\ k \\ l \end{pmatrix}_{op} + \begin{pmatrix} h \\ k \\ l \end{pmatrix}_{co} . \qquad (14)$$

In connection with structural phase transitions, the argument can be extended to the case of superlattice reflections. When indexing is based on the fundamental lattice, at least one of *h, k, l* of the superlattice reflections is half integer, or $1/n$ integer in general.

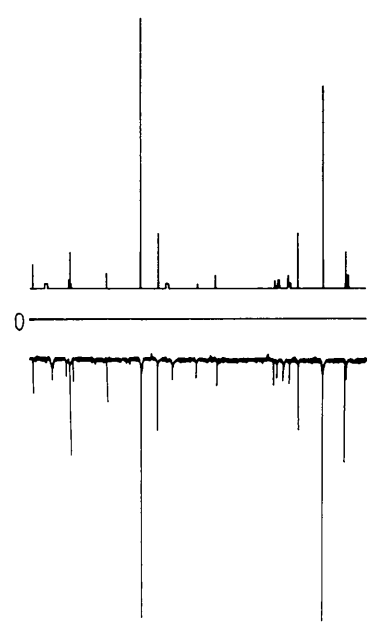

Fig. 6. Pattern of ψ scanning for 002 of GaAs with Cu $K\alpha_1$. The lower part is that of the experiment (Chang & Post, 1975).

Therefore, double diffractions with operative and cooperative points of the fundamental lattice cannot introduce any intensity to the superlattice reflection; the intensity can be transferred there only when either or both the operative and cooperative reflections are those of the superlattice.

This means that the intensity of the double diffraction is only of the order of 10^{-2}-10^{-3} of that of the superlattice reflection concerned even when the other reflection involved is of the fundamental lattice. Consequently, in usual conditions, double diffraction does not bring any detectable intensity to superlattice points. The situation can be seen from (11): if N_h is very small as in the present case, the only contribution is that of $r^2 N_{op} N_{co}$, which is not significant unless both of N_{op} and N_{co} are large, or at least very much larger than N_h.

If there is any doubt about multiple diffraction, the comparison of experiment and simulation of the ψ (or λ) scanning will be very useful. Since weak intensities and loss of them can result from spurious processes, one must be careful in attributing them to multiple diffraction. In fact, in the literature of multiple diffraction, we often find erroneous assignment of peaks; two examples are explicitly shown in Table 1. Moreover, in some cases, attribution to multiple diffraction has been made without showing the assignment of contributing processes.

It should be emphasized that the agreement between the present simulation and the published experimental data shows the validity of the kinematical theory to multiple diffraction (*n*-beam interaction) processes. This is quite contrary to what is stated in textbooks and previous papers: that is, it has been accepted that the *n*-beam interaction should be treated in terms of the dynamical theory. Discussion of this problem is not within the scope of the present paper.

In consequence of the present study, however, the discussion of *n*-beam interactions becomes clear and easy to understand. Moreover, the calculation can be carried out even by microcomputers.

In conclusion, it is to be hoped that the simulation of *n*-beam interactions will be applied to various cases in order to confirm the validity.

The authors are grateful to Professor N. Kato for very encouraging comments on the applicability of the kinematical theory to the present problem. The work is supported by Grant-in-Aid for Scientific Research from the Ministry of Education, Science and Culture.

APPENDIX *A*

Here we examine the effect of the four-beam interaction. The two operative points of the Ewald sphere will be denoted by h_{op1} and h_{op2}. The simultaneous

equations corresponding to (7) for the three-beam case can be given as follows:

$$I_{\mathbf{h}} = (I_0 - I_{\mathrm{op1}} - I_{\mathrm{op2}}) r_{\mathbf{h}} N_{\mathbf{h}} \qquad (A.1a)$$

$$I_{\mathrm{op1}} = (I_0 - I_{\mathbf{h}} - I_{\mathrm{op2}}) r_{\mathrm{op1}} N_{\mathrm{op1}} \qquad (A.1b)$$

$$I_{\mathrm{op2}} = (I_0 - I_{\mathbf{h}} - I_{\mathrm{op1}}) r_{\mathrm{op2}} N_{\mathrm{op2}}, \qquad (A.1c)$$

where the quantities with the additional suffixes 1 and 2 correspond to $\mathbf{h}_{\mathrm{op1}}$ and $\mathbf{h}_{\mathrm{op2}}$, respectively. After (A.1) has been solved, the intensity escaping from $\mathbf{h}$ to $\mathbf{h}_{\mathrm{op1}}$ and $\mathbf{h}_{\mathrm{op2}}$ *via* relevant cooperative points can be written as $(r_{\mathrm{co1}} N_{\mathrm{co1}} + r_{\mathrm{co2}} N_{\mathrm{co2}}) I_{\mathbf{h}}$, with that coming to $\mathbf{h}$ from $\mathbf{h}_{\mathrm{op1}}$ and $\mathbf{h}_{\mathrm{op2}}$ as $(r_{\mathrm{co1}} N_{\mathrm{co1}} I_{\mathrm{op1}} + r_{\mathrm{co2}} N_{\mathrm{co2}} I_{\mathrm{op2}})$. Following the discussion in § 2.2, and neglecting the terms of third and fourth order in r, we find the relation corresponding to (10) as follows:

$$\begin{aligned}(I_h)_{\mathrm{obs}}/I_0 \simeq {} & rN_{\mathbf{h}}\{1 - r(N_{\mathrm{op1}} + N_{\mathrm{op2}})\} \\ & - r^2 N_{\mathbf{h}}(N_{\mathrm{co1}} + N_{\mathrm{co2}}) \\ & + r^2(N_{\mathrm{op1}} N_{\mathrm{co1}} + N_{\mathrm{op2}} N_{\mathrm{co2}}). \qquad (A.2)\end{aligned}$$

Comparing this equation with (10), and extending the discussion to the case of the existence of three or more operative points, we find that the effect of the n-beam interaction can be described by summing up the effects of independent three-beam interactions arising from pairs of h and individual operative points, provided that r is still small for third and further diffractions.

APPENDIX *B*

The polarization factor for three-beam cases is described in the following. The quantity ρ given by Zachariasen (1965) can be expressed as

$$\tan\rho = \tan\chi \sin(\phi + 2\theta), \qquad (B.1)$$

where χ and ϕ are the angles made by the projection of I_{op} on to the $I_0 I_{\mathbf{h}}$ plane with I_{op} and I_0, respectively (Fig. 1). According to Azaroff (1955),

$$\begin{aligned}p_{\mathrm{co}} = {} & \{(\cos^2\beta\cos^2\rho + \sin^2\rho)\cos^2\alpha \\ & + \cos^2\beta\sin^2\rho + \cos^2\rho\}/(1 + \cos^2\beta), \qquad (B.2)\end{aligned}$$

where α and β are the angles made by I_{op} with $I_{\mathbf{h}}$ and I_0 respectively. p_{co}^* will be obtained by replacing β by 2θ. The total p factors are consequently $p_{\mathbf{h}} p_{\mathrm{co}}^*$ and $p_{\mathrm{op}} p_{\mathrm{co}}$ for *Aufhellung* and *Umweganregung*, respectively.

References

AZAROFF, L. V. (1955). *Acta Cryst.* **8**, 701–704.
CHANG, S. L. & POST, B. (1975). *Acta Cryst.* A**31**, 832–835.
COPPENS, P. (1968). *Acta Cryst.* A**24**, 253–257.
LIPSON, H. & COCHRAN, W. (1953). *The Determination of Crystal Structures*, p. 32. New York: Cornell Univ. Press.
MATSUMOTO, T. (1983). *Kōbutsu-gaku Zasshi* (*J. Miner. Soc. Jpn*), **16**, 99–108 (in Japanese).
MOON, R. M. & SHULL, C. G. (1964). *Acta Cryst.* **17**, 805–812.
PANKE, D. & WÖLFEL, E. (1968). *J. Appl. Cryst.* **1**, 255–257.
POST, B. (1975). *Acta Cryst.* **8**, 452–456.
RENNINGER, M. (1937). *Z. Phys.* **106**, 141–176.
SAMUELSON, E. J. (1974). *J. Phys. C*, **7**, L115–L117.
SAMUELSON, E. J. & STEINSVOLL, O. (1975). *J. Phys. C*, **8**, L427–L429.
SASAKI, S. & MATSUMOTO, T. (1977). *Proc. Jpn Acad.* **53B**, 84–89.
SASAKI, S., MATSUMOTO, T. & SAWADA, C. (1981). *Phys. Chem. Miner.* **7**, 260–267.
SHIRANE, G., CHIKAZUMI, S., AKIMITSU, J., CHIBA, K., MATSUI, M. & FUJII, Y. (1975). *J. Phys. Soc. Jpn*, **39**, 949–957.
THOMPSON, P. & GRIMES, N. W. (1977). *J. Appl. Cryst.* **10**, 369–371.
ZACHARIASEN, W. H. (1965). *Acta Cryst.* **18**, 705–710.

Acta Cryst. (1985). A**41**, 133–142

Tensor X-ray Optical Properties of the Bromate Ion

BY DAVID H. TEMPLETON AND LIESELOTTE K. TEMPLETON

Materials and Molecular Research Division, Lawrence Berkeley Laboratory and Department of Chemistry, University of California, Berkeley, California 94720, *USA*

(*Received* 6 *July* 1984; *accepted* 17 *September* 1984)

Abstract

Linearly polarized synchrotron radiation has been used to observe X-ray dichroism of the bromate ion near the bromine K edge by transmission absorption spectroscopy using a crystal of potassium bromate, and to measure the anomalous scattering of bromine and its anisotropy in diffraction experiments with sodium bromate. The principal values of f'' are as high as 12 and 17 electrons atom^{-1} and of f' as low as -13 and -15 for polarization respectively parallel and perpendicular to the threefold axis. The anisotropy is as much as 6·6 for f'' and 4·6 for f', or a few percent more after correction for thermal motion and for incomplete polarization of the beam. A consequence of this large anisotropy is that reflec-

0108-7673/85/020133-10$01.50